Link-Budget Analysis of Dynamic Impairments on E-/W-Band High Through-Put Feeder Links for Future VLEO Small Satellites

1st Mark J. Neff
Institute of Robust Power Semiconductor Systems
University of Stuttgart
Stuttgart, Germany
mark.neff@ilh.uni-stuttgart.de

2nd Benjamin Schoch
Institute of Robust Power Semiconductor Systems
University of Stuttgart
Stuttgart, Germany
benjamin.schoch@ilh.uni-stuttgart.de

3rd Ingmar Kallfass
Institute of Robust Power Semiconductor Systems
University of Stuttgart
Stuttgart, Germany
ingmar.kallfass@ilh.uni-stuttgart.de

***Abstract*—This work describes the dynamic link-budget analysis of high-throughput feeder links at E- and W-band (71 GHz to 76 GHz and 81 GHz to 86 GHz) for small satellites in very low Earth orbit, accounting for the dynamic impairments caused by rapidly varying link geometries. The link budgets are estimated for satellite zenith passes at 200 km and 450 km satellite altitude, and for a 90°-inclined orbit, with a ground station located in the urban area of Stuttgart, Germany. All available ITU recommendations for atmospheric attenuation are considered, and the transmitter system is modeled at a high level using state-of-the-art E-band components. The estimated link budgets are evaluated based on the achieved channel capacity and total transmitted data volume for three different annual availabilities 90 %, 95 %, and 99 %, achieving up to 39 Gbit/s.**

***Index Terms*—link budget, millimeter wave communication, satellite, VLEO, Wideband.**

I. Introduction

Satellites in Earth's closest orbit, the very low earth orbit (VLEO) (200 km to 450 km), are attracting increasing attention because their proximity to the surface improves spatial resolution, strengthens link margins, lowers required transmit power, and reduces latency. These advantages that are especially valuable for Earth observation (EO), communications, and advanced-sensor payloads. The high orbital velocities in VLEO result in a high number of orbits per day, enabling optical EO payloads to cover more ground in a shorter period and capture more detailed images. At the same time, transmitting this large data accumulation from VLEO to Earth in a timely manner is challenging, as the high orbital velocity and rapidly changing geometry produce very short ground-contact windows and a large dynamic range. Maximizing communication throughput during these very short contact windows is therefore essential to ensure timely offload of gathered data or to offload data from satellites connected via inter-satellite links (ISL), which at the time do not have access to a ground station [1].

Commercial optical communication systems in the 1 U to 2 U class offer comparatively moderate to high data rates, low per-bit power consumption, and superior theoretical bandwidth efficiency compared to radio frequency (RF) systems, while alleviating potential licensing issues. Optical systems in this size class currently operate in the 0.01 Gbit/s to 1 Gbit/s range for downlink operation [2], [3], with uplink data rates typically significantly lower and constrained by pointing accuracy and aperture size. Additionally, in the absence of site diversity, optical communication systems are highly susceptible to atmospheric effects, particularly cloud cover and fog, which can lead to complete link outages. In contrast, millimeter-wave (mmW, 30 GHz to 300 GHz) systems, while also affected by weather phenomena such as rain attenuation, generally maintain connectivity under more adverse conditions, albeit with reduced link margins and data rates compared to clear-sky operation. This trade-off between peak throughput and link availability is especially critical in VLEO scenarios, where short contact durations make maximizing communication availability essential.

While commercial LEO constellations presently use K/Ka-band (17.7 GHz to 21.2 GHz, 27.5 GHz to 31 GHz) for feeder links, the industry is shifting toward millimeter-wave bands. The next higher frequency bands, the Q- and V-bands (37.5 GHz to 42.5 GHz, 47.2 GHz to 51.4 GHz) and, more recently, the E-band (downlink 71 GHz to 76 GHz, uplink 81 GHz to 86 GHz) have been allocated for satellite services by the International Telecommunications union (ITU) [4]. These bands offer a larger continuous bandwidth than the K/Ka-band, and the approval of E-band usage for

This work is funded by the Deutsche Forschungsgemeinschaft (DFG, German Research Foundation) – Project-ID 516238647 – SFB 1667 (ATLAS - Advancing Technologies of Very Low-Altitude Satellites)

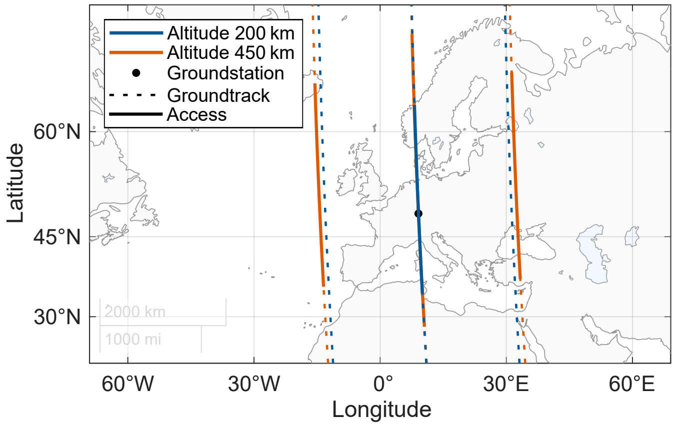

Fig. 1. Map of the ground track and visibility of the satellites at 200 km and 450 km altitude and 90 % inclination over the ground station in Stuttgart.

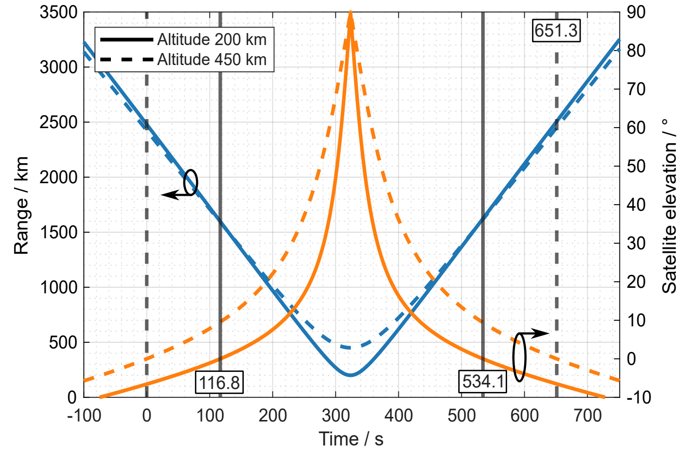

Fig. 2. Simulated range and elevation over time for a zenith pass of the satellites at 200 km and 450 km altitude.

SpaceX's second-generation Starlink and the feasibility studies for LEO [5], [6] underline the growing interest in these higher-frequency, wide-bandwidth channels from both industry and academia. Consequently, a rigorous link-budget analysis that accounts for the dynamic impairments of VLEO is essential to assess the achievable data rates of high-throughput E/W-band feeder links for future small-satellite missions.

This work compares dynamic link budget analyses for ultra-high data rate satellite communication in the mmW E- and W-bands. It analyzes the dynamic effects and link impairments encountered at VLEO orbit heights.

II. Orbit Scenario

The reference scenario for this work is a sustained VLEO EO mission at two different orbital altitudes: the lower edge at 200 km and the upper edge at 450 km, to compare the E-band link at the two extremes of the VLEO. An arbitrary fully circular 90 % inclined orbit is chosen for a full coverage of the earths surface for this hypothetical EO scenario. Satellite orbit simulation is performed in MATLAB using the Satellite Communication Toolbox and the SGP4 propagator. In mmW satellite communication, one of the major performance factors is the local climate at the ground station location. The ground station in this work is modeled after the E-band ground station developed in the demonstrator mission EIVE [4] and is located on the Stuttgart University campus in a mid-latitude temperate climate in southern Germany, as shown in Fig. 1. Three consecutive orbits of both satellites at different altitudes are shown in Fig. 1, with the portions of the ground track where the satellite is over the horizon of the ground station highlighted by a solid line. Figure 1 also shows the significant reduction in this section length where access can be established for the lower orbit.

This reduction translates to reduced access time, as shown in the range and elevation angle plot in Fig. 2. For the chosen inclination, a zenith pass of a satellite in 450 km orbit results in an access time, i.e., elevation angle over 0° is 651.3 s while the time spent at higher elevation is a fraction of this time. For the lower 200 km orbit, the total access time reduces to just 417.3 s, with the time spent at higher elevations further reduced.

III. Dynamic Effects

The rapid change in both range and elevation largely dictates the communication-related dynamic effects. For different orbital altitudes, one of the more apparent effects is the increase in minimum free space path loss (FSPL) shown in Fig. 3 a). In E-band the FSPL increases from around 8 dB at 150 km to around 19 dB at 2000 km shown in Fig. 3 a) in comparison to the more established K-band. Interestingly, however, the delta FSPL, which is the difference between the maximum FSPL at the horizon and the minimum FSPL experienced at zenith for one satellite pass, is independent of frequency and solely depends on the satellite's altitude. This dynamic range is important to consider when designing a receiver, as, from geometry alone, the input signal will vary by up to 19.5 dB at 150 km orbit altitude during one zenith pass.

The reduction in access time and resulting narrowing of the peak in elevation angle over time seen in Fig. 2 has significant implications for the positioning and tracking of the ground station and satellite antenna. Shown in Fig. 3 b) is the peak angular velocity of the satellite relative to the ground station, which increases significantly with decreasing orbital height, with the angular velocity at 150 km being approximately three times that at 450 km. Achieving these high tracking speeds could proof difficult for large antennas with several meters in diameter.

A higher relative velocity between the satellite and the ground station at lower satellite altitudes also means a larger Doppler shift is encountered, especially at the very high frequencies in the E-band. Both the maximum Doppler shift and peak Doppler rate are shown in Fig. 3 c) in comparison to K-band, and as expected, both are significantly higher in the higher frequency E-band and at lower orbit heights. At its maximum, Doppler shifts around 2 MHz and Doppler rates up to 100 kHz/s are encountered for the lowest VLEO orbit heights. At the same time, these comparatively high values can be compensated for by modern systems. However, they should

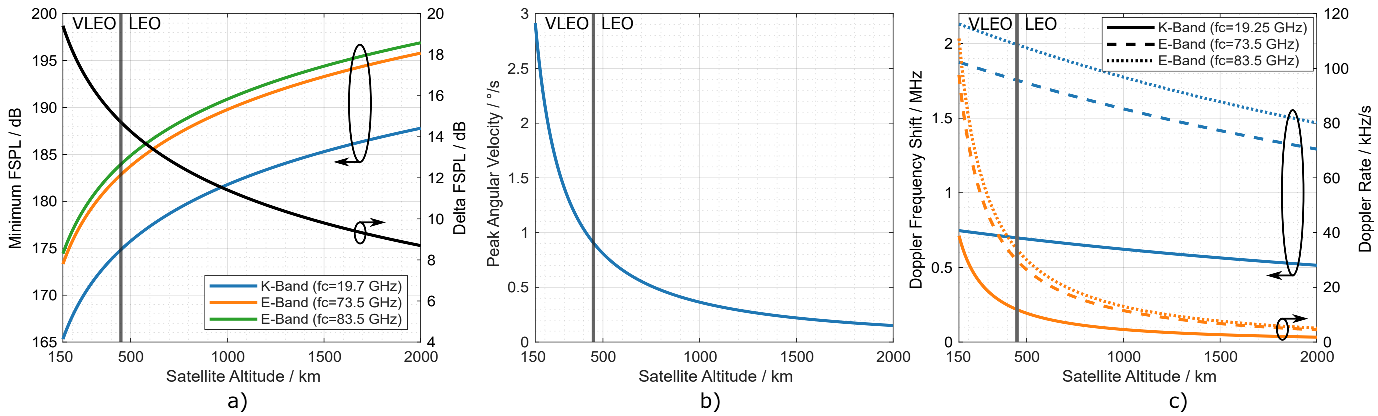

Fig. 3. a) The minimum FSPL and delta between the minimum and maximum FSPL, b) the peak angular velocity, and c) the maximum Doppler shift and peak Doppler rate for zenith passes at different orbit heights and center frequencies.

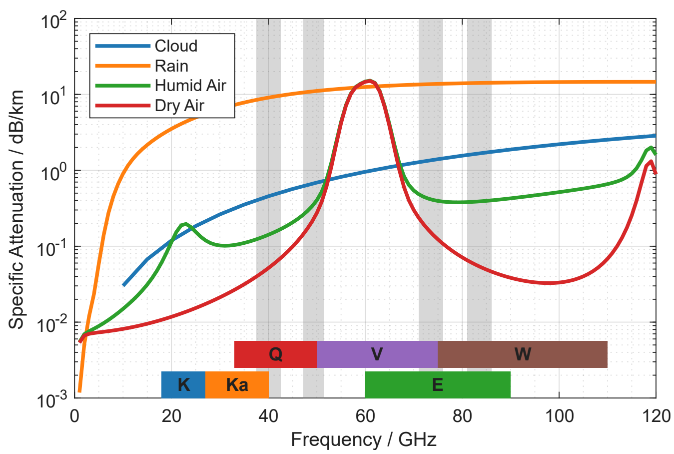

Fig. 4. Specific attenuation of different atmospheric effects over frequency, showing the frequency range of different frequency bands as well as the spectrum allocated for satellite communication in dark gray.

be considered early in the system design process to ensure fast signal acquisition times within the very short timeframe of a VLEO satellite access window.

IV. Atmospheric Effects

One major consideration in mmW communication is the increased attenuation caused by atmospheric effects, such as rain, clouds, gases, and density variations along the communication link. This frequency related increase in specific attenuation can be seen in Fig. 1, which shows the frequency dependence of cloud, rain, and gaseous attenuation per kilometer for an atmospheric pressure of 101.3 kPa, a water vapor density of 7.5 g/m^3, a cloud liquid water content of 0.5 g/m^3, a temperature of 15 °C, and a rain rate of 20 mm/h. The dark gray areas indicate the locations of the mmW satellite communication bands, which lie symmetrically to the left and right of the oxygen resonance peak around 60 GHz, where the gaseous attenuation spikes to above 10 dB/km. In the rapidly varying link geometry of VLEO, the increase in atmospheric attenuation is exacerbated, as almost every atmospheric effect is elevation-angle dependent and more time is spent at shallow elevation angles, where the path through the atmosphere is

TABLE I
ITU recommendations used for propagation and link budget modeling.

	Recom.	Ref.	Valid Freq. (GHz)
Radio refractive index	ITU-R P.453-14	[8]	All
Noise & Scintillation	ITU-R P.618-14	[7]	All / 4–55
Gas attenuation	ITU-R P.676-13	[9]	1–1000
Reference atmosphere	ITU-R P.835-7	[10]	All
Water vapour density	ITU-R P.836-6	[11]	All
Precipitation Characteristics	ITU-R P.837-7	[12]	All
Specific rain attenuation	ITU-R P.838-3	[13]	1–1000
Rain height model	ITU-R P.839-4	[14]	All
Cloud Attenuation	ITU-R P.840-9	[15]	1–200
Mean surface temperature	ITU-R P.1510-1	[16]	All
Topography of earth	ITU-R P.1511-3	[17]	All

longer than at zenith, resulting in higher total attenuation. The total atmospheric attenuation can be estimated as described in ITU-R P.618-14 [7] as:

$$L_{\text{atm,dB}} = L_{\text{gas,dB}} + \sqrt{(L_{\text{rain,dB}} + L_{\text{cloud,dB}})^2 + L^2_{\text{scint,dB}}}, \quad (1)$$

where the total elevation dependent atmospheric attenuation $L_{\text{atm,dB}}$ is composed of the gaseous attenuation $L_{\text{gas,dB}}$, precipitation attenuation $L_{\text{rain,dB}}$, and scintillation fading $L_{\text{scint,dB}}$ due to turbulent layers in the atmosphere. The simulation automatically adjusts all location-specific atmospheric parameters to ITU-recommended climate data for the ground station location. The sub-attenuations are evaluated for a given annual exceedance probability p, where an exceedance of 1 % corresponds to an annual availability of 99 %. This implies that the atmospheric conditions assumed in the attenuation calculation are exceeded for only 1 % of the time over the course of a year. The overview of the implemented ITU recommendations with their valid frequency ranges is shown in Table I. Only one model, the scintillation model described in ITU-R P.618-14, is not valid at E-band frequencies but is applied in this work due to a lack of widely accepted alternatives.

V. Hardware

Despite the demand for higher data rates, E-band hardware for satellite communication remains a niche technology. There-

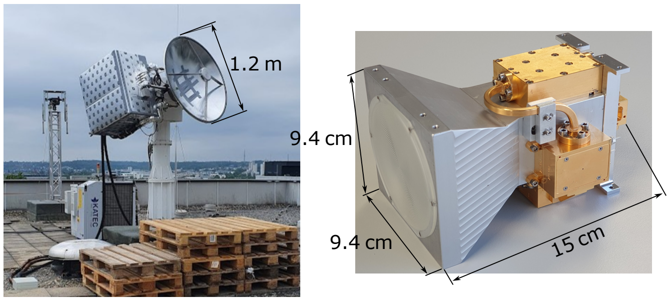

a) b)

Fig. 5. Pictures and dimensions of a) the ground segments and b) the space segment of the feasibility study EIVE [4] used as the reference hardware in this work.

fore, as a reference communication hardware, the LEO satellite mission EIVE [4] was chosen to test the effects and capabilities in VLEO. Focussing on the most relevant components and hardware metrics for the link budget, the ground segment of the EIVE mission consisted of a mechanically steered 1.2 m Cassegrain antenna system with multimode monopulse tracking [4] and a low noise amplifier (LNA) with a 2 dB noise figure [18] shown in Fig. 5 a). Typically, electronically steered phased array antennas, both on satellite and on the ground, easily meet the fast angular velocity requirements for antenna tracking at lower orbits, as seen in Fig. 3 b). However, phased arrays for mmWave satellite communication are constrained by the need for very high antenna gains (driving large element counts), increased losses in the RF distribution network at higher frequencies, limited available aperture in small satellite form factors, and the added challenges of power consumption, thermal management, and complex beamforming hardware. With this in mind, we are unaware of a viable phased-array antenna for satellite communication in the E-band. The tracking requirements are also met by a light, compact reflector antenna with a fast mechanical positioner, as seen in [4].

The 1.5 U satellite transmitter payload of the EIVE mission shown in Fig. 5 b), consists of a corrugated horn antenna, a dielectric lens with a 9 cm aperture, and a solid-state power amplifier (SSPA) with 2 W (33 dBm) transmit power [19], which is well aligned with the state of the art of compact SSPAs [4], [19] and commercially available options [20]. This limited output power at high mmW frequencies is, hardware-wise, one of the most significant limiting factors complicating communication, as above the Ka-band, the achievable RF power saturates at a few watts for compact, small-satellite power amplifiers. Since the EIVE mission was focused exclusively on the downlink 71 GHz to 76 GHz, it is assumed in this work that the hardware is modified for duplex operation by adding the LNA from the ground section to the payload and the payload SSPA to the ground station, ignoring the additional mixers required for down- and up-conversion in the payload and on ground, respectively. For reference the EIVE payload consisted of the transmitter frontend with a power consumption of around 36 W and a signal generator board consuming between 10 W and 25 W [4] putting the proposed duplex frontend in this work to around 60 W, which

TABLE II
SUMMARY OF THE COMMUNICATION SYSTEM HARDWARE PARAMETERS USED IN THE LINK BUDGET FOR BOTH UP- AND DOWNLINK.

	Unit	**E-band** Downlink	**E-band** Uplink
Center freq.	GHz	73.5	83.5
Bandwidth	GHz	5	
GS aperture diam.	m	1.2	
GS antenna gain	dBi	57.5	58.6
Sat. aperture diam.	m	0.09	
Sat. antenna gain	dBi	35	36
Transmit power	dBm	33	
LNA noise figure	dB	2	
Feed loss	dB	1	
Polarization loss	dB	0.5	
Pointing loss	dB	1	

is significantly higher than the < 35 W of peak power that comparably sized optical terminals claim [2]. The same SSPA which is used in the payload is assumed for the ground station in this work for simplicity, and as the uplink transmit power is typically constrained by regulations, even though higher-power amplifiers, such as traveling-wave tube amplifiers (TWTA) or large SSPAs, are available in the chosen frequency bands, their size, weight, and power consumption are a significant trade-off when designing a compact small satellite and highly dynamic and compact mechanically steered ground station.

The antenna gain G in dBi of the lens antenna system and the Cassegrain antenna system depends both on the aperture diameter D and the wavelength λ according to the standard aperture efficiency model [21]:

$$G = 10 \log_{10} \left(\eta \cdot \left(\frac{\pi \cdot D}{\lambda} \right)^2 \right) \tag{2}$$

where the aperture efficiency η is assumed to be 65 % in this work accounts for dielectric and illumination losses. Since the up- and down-link frequencies are 10 GHz apart in the E-band, in the absence of measurement data for both bands, it is important to calculate the antenna gain in both bands to account for the frequency-dependent increase of the antenna gain in the link budget. An overview of all hardware-related link budget assumptions used in this work is shown in Table II. Realistic implementation losses for mmW feeder links include feed losses on the order of 0.5 dB to 1.5 dB, polarization mismatch losses of approximately 0.2 dB to 0.5 dB, and pointing losses ranging from 0.5 dB to 1.5 dB depending on platform stability and beamwidth, with pointing errors typically representing the dominant impairment in high-frequency, narrow-beam systems. The assumed losses are also shown in Table II.

VI. LINK BUDGET

In its simplest form, the link budget is the addition and subtraction of all losses and gains in a transmission system to calculate the input power at the receiver, $P_{\mathrm{RX,dBm}}$. It typically can be expressed as [6]:

$$P_{\mathrm{RX,dBm}} = P_{\mathrm{TX,dBm}} + G_{\mathrm{TX,dBi}} + G_{\mathrm{RX,dBi}} - \mathrm{FSPL_{dB}} - L_{\mathrm{atm,dB}} - L_{\mathrm{TX/RX,dB}} \tag{3}$$

where $P_{\mathrm{TX,dBm}}$ is the transmitter output power, which is added to $G_{\mathrm{RX,dBi}}$ and $G_{\mathrm{TX,dBi}}$ the antenna gains on the receive ant transmit side. The losses, i.e., $\mathrm{FSPL_{dB}}$, the atmospheric loss $L_{\mathrm{atm,dB}}$, and other losses on the transmit and receive side $L_{\mathrm{TX/RX,dB}}$ like the feed, polarization, and pointing losses shown in Table II are subsequently subtracted. Subtracting the total noise in dB from the received power results in the carrier to noise ratio:

$$\left(\frac{C}{N}\right)_{\mathrm{dB}} = P_{\mathrm{RX,dBm}} - 10\log_{10}\left(k \cdot T_{\mathrm{sys}} \cdot B\right) \tag{4}$$

where k is the Boltzmann constant, T_{sys} is the total system noise temperature and B is the bandwidth of the communication link. The total system noise temperature, specifically the antenna noise temperature, is elevation-angle-dependent and not reciprocal with the link direction; i.e., earth-to-space links will have a different antenna noise temperature than space-to-earth links. This noise temperature is dependent on the sky noise temperature in the field of view of the receive antenna and can be estimated using [7], [9], [22].

The theoretical maximum data rate of a communication channel, the channel capacity C, according to the Shannon-Hartley theorem, can be estimated for an additive white Gaussian noise channel using the bandwidth and the carrier-to-noise ratio as follows:

$$C = B\log_2\left(1 + \left(\frac{C}{N}\right)_{\mathrm{lin}}\right) \tag{5}$$

resulting in the channel capacity in bits per second. This represents the theoretical upper bound on the achievable data rate for a given bandwidth and signal-to-noise ratio. It assumes ideal coding and modulation schemes and arbitrarily low error probability, and is therefore not directly achievable in practical systems. In practice, achievable rates fall below this bound due to finite block lengths, implementation losses, and channel estimation errors. Nevertheless, it provides a useful benchmark for evaluating link performance independently of specific communication protocols and implementation details.

Figure 6 shows the channel capacity over a zenith pass estimated for the satellite at 200 km altitude for both downlink at a center frequency $fc = 73.5\,\mathrm{GHz}$ and uplink at $fc = 83.5\,\mathrm{GHz}$. As expected, for more adverse weather conditions encountered for lower exceedance probabilities p, the overall channel capacity drops to a peak capacity in zenith of 21.8 Gbit/s for 73.5 GHz and 25.5 Gbit/s for 83.5 GHz. The increase in channel capacity with increasing center frequency at a constant bandwidth of 5 GHz stems from the fixed antenna size, which results in an increase in antenna gain as wavelengths shrink (i.e., frequency increases). With increasing exceedance probability, both the maximum channel capacity and the duration of the access period during which E-band communication exceeds Gbit/s increase (see Table III),

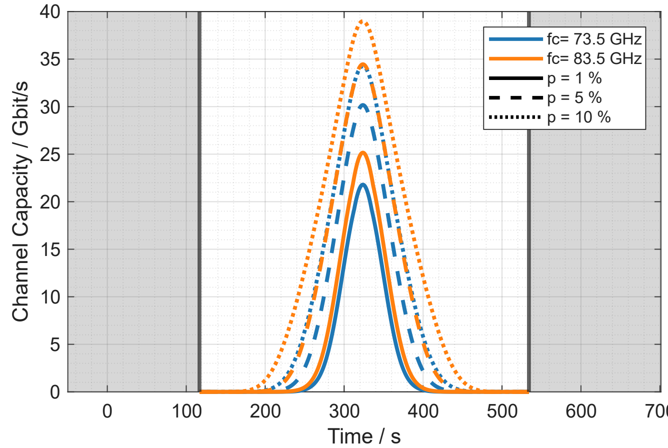

Fig. 6. Calculated channel capacity for both E-band up-and down-link for different annual exceedance probabilities p for an orbit altitude of 200 km with the access period highlighted in white.

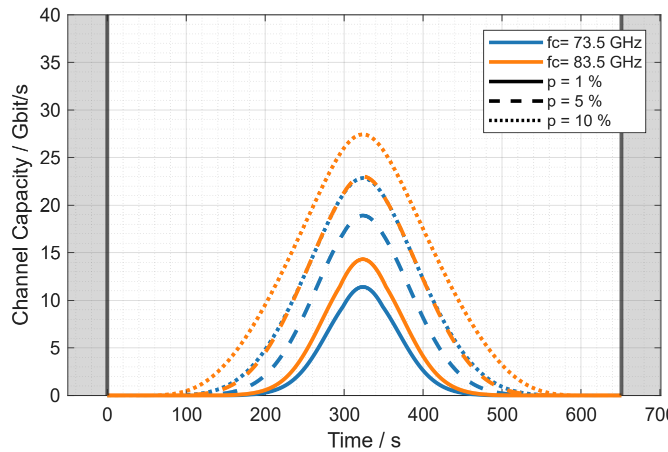

Fig. 7. Calculated channel capacity for both E-band up-and down-link for different annual exceedance probabilities p for an orbit altitude of 450 km with the access period highlighted in white.

resulting in a higher total data volume transmitted during a single ideal zenith pass. The highest peak channel capacity is achieved for $p = 10\,\%$, $fc = 83.5\,\mathrm{GHz}$ with 39.0 Gbit/s and a total of 577 GB transmitted.

Increasing the orbit height to 450 km increases the FSPL and therefore reduces the peak capacity compared to the lower orbit as shown in Fig. 7. However, even though the peak capacity is reduced compared to the 200 km satellite, the peak in channel capacity is broader over time and therefore achieves similiar or higher total transmitted data volumes with the highest value achieved for $p = 10\,\%$, $fc = 83.5\,\mathrm{GHz}$ with 27.4 Gbit/s and a total of 709.4 GB. This difference between the scenarios shown in Fig. 6 and Fig. 7 shows how important it is to maximize the communication time even if very high channel capacities are achieved to maximize the total transmitted data volume, especially considering, that most orbits will not result in a zenith pass of a singular ground station and therefore reduces the expectable data rate significantly.

TABLE III
OVERVIEW OF THE ACHIEVED PEAK DATA RATES AND TOTAL TRANSMITTED DATA VOLUME FOR THE INVESTIGATED ORBIT HEIGHTS AND ANNUAL EXCEEDANCE PROBABILITIES.

Altitude (km)	**fc** (GHz)	**Exc. prob.** (%)	**Max. capacity** (Gbit/s)	**Total data** (GB)
200	73.5	1	21.8	165.0
		5	30.2	309.4
		10	34.3	417.1
	83.5	1	25.2	208.0
		5	34.5	409.2
		10	39.0	577.0
450	73.5	1	11.4	157.2
		5	18.9	346.9
		10	22.8	491.5
	83.5	1	14.3	214.0
		5	23.0	486.0
		10	27.4	709.4

VII. CONCLUSION

In this paper, we present a thorough dynamic link-budget analysis of E-band high-throughput feeder links for VLEO small satellites, accounting for dynamic impairments at low altitudes and at high mmW frequencies. For two exemplary orbit heights of 200 km and 450 km at a 90° inclination, multi Gbit/s data links peaking at 11.4 Gbit/s to 34.5 Gbit/s are theoretically achievable using compact state-of-the-art ground station hardware and a small 1.5 U satellite transceiver payload even in adverse weather conditions at a 90 %, 95 %, and 99 % annual availability. The achieved data rate at a compact size for annual availability indicates that compact E-band transceivers may significantly outperform similarly sized optical transmitters, though at the cost of increased power consumption.

REFERENCES

[1] S. Yang, J. Sun, H. Lu, S. Cheng, S. Wang, and W. Sun, "Advantage analysis of spaceborne sar imaging in very low earth orbit: A case study of haishao-1," *Remote Sensing*, vol. 17, no. 22, 2025.

[2] Tesat-Spacecom GmbH & Co. KG, "SCOT20 Smallsat Optical Communication Terminal Datasheet," Tesat-Spacecom GmbH & Co. KG, Datasheet, 2024, accessed: 2026-04-29. [Online]. Available: https://satsearch.s3.eu-central-1.amazonaws.com/datasheets/datasheet-tesat-spacecom-gmbh-co-kg-scot20-smallsat-optical-communication-terminal-fl1jn4.pdf

[3] D. Muhire, D. Stepanova, S. Santra, P. Baranwal, M. Romero, R. Amrutkar, S. Bonnart, D. Jha, and A. Zucherman, "Optical communications for small satellites: A review of pointing strategies & requirements optimization," *Proceedings of the International Astronautical Congress*, vol. IAC-2020, 2020, paper IAC-20-B2.4.1.

[4] I. Kallfass, L. Manoliu, B. Schoch, M. Koller, S. Klinkner, J. Freese, A. Tessmann, and R. Henneberger, "Towards the exploratory in-orbit verification of an e/w-band satellite communication link," in *2021 IEEE MTT-S International Wireless Symposium (IWS)*, 2021, pp. 1–3.

[5] U. J. Lewark, J. Antes, J. Walheim, J. Timmermann, T. Zwick, and I. Kallfass, "Link budget analysis for future e-band gigabit satellite communication links (71–76 and 81–84 ghz)," *CEAS Space Journal*, vol. 4, no. 1, pp. 41–46, Jun 2013. [Online]. Available: https://doi.org/10.1007/s12567-013-0030-0

[6] B. Schoch, L. Manoliu, J. Keim, S. Chartier, S. Klinkner, and I. Kallfass, "Link-Budget Analysis of W- and E-Band Satellite Services," in *Proc. 25th Ka and Broadband Conference*, 2019.

[7] "Propagation Data and Prediction Methods Required for the Design of Earth-Space Telecommunication Systems," International Telecommunication Union (ITU-R), Tech. Rep. P.618-14, 2023.

[8] "The Radio Refractive Index: Its Formula and Refractivity Data," International Telecommunication Union (ITU-R), Geneva, Switzerland, Tech. Rep. P.453-14, 2019.

[9] "Attenuation by Atmospheric Gases," International Telecommunication Union (ITU-R), Geneva, Switzerland, Tech. Rep. P.676-13, 2022.

[10] "Reference Atmosphere," International Telecommunication Union (ITU-R), Geneva, Switzerland, Tech. Rep. P.835-7, 2024.

[11] "Water Vapour: Surface Density and Total Columnar Content," International Telecommunication Union (ITU-R), Geneva, Switzerland, Tech. Rep. P.836-6, 2017.

[12] "Characteristics of Precipitation for Propagation Modelling," International Telecommunication Union (ITU-R), Geneva, Switzerland, Tech. Rep. P.837-7, 2017.

[13] "Specific Attenuation Model for Use in Prediction Methods," International Telecommunication Union (ITU-R), Geneva, Switzerland, Tech. Rep. P.838-3, 2005.

[14] "Rain Height Model for Prediction Methods," International Telecommunication Union (ITU-R), Geneva, Switzerland, Tech. Rep. P.839-4, 2013.

[15] "Attenuation Due to Clouds and Fog," International Telecommunication Union (ITU-R), Geneva, Switzerland, Tech. Rep. P.840-9, 2023.

[16] "Mean Surface Temperature," International Telecommunication Union (ITU-R), Geneva, Switzerland, Tech. Rep. P.1510-1, 2017.

[17] "Topography for Earth-Space Propagation Modelling," International Telecommunication Union (ITU-R), Geneva, Switzerland, Tech. Rep. P.1511-3, 2024.

[18] A. Tessmann, A. Leuther, C. Schwoerer, H. Massler, S. Kudszus, W. Reinert, and M. Schlechtweg, "A coplanar 94 ghz low-noise amplifier mmic using 0.07 /spl mu/m metamorphic cascode hemts," in *IEEE MTT-S International Microwave Symposium Digest, 2003*, vol. 3, 2003, pp. 1581–1584 vol.3.

[19] E. Ture, S. Leone, P. Brückner, R. Quay, and O. Ambacher, "High-power (¿2 w) e-band pa mmic based on high efficiency gan-hemts with optimized buffer," in *2019 IEEE MTT-S International Microwave Symposium (IMS)*, 2019, pp. 1407–1410.

[20] Filtronic plc, "SSPAs: The Power Behind Long-Range Datalinks," https://filtronic.com/wp-content/uploads/2025/12/9922-Filtronic-SSPA-Brochure.pdf, 2025, product brochure, accessed Mar. 20, 2026.

[21] J. L. Volakis, *Antenna Engineering Handbook*. McGraw-Hill, 2007.

[22] B. Butler, "ngVLA Memo #96: ngVLA Antenna Noise Temperature Calculation," National Radio Astronomy Observatory (NRAO), Tech. Rep. ngVLA Memo 96, 2018.